IEEE Access
Multidisciplinary | Rapid Review | Open Access Journal

Received 18 December 2023, accepted 8 January 2024, date of publication 17 January 2024, date of current version 25 January 2024.

Digital Object Identifier 10.1109/ACCESS.2024.3355055

RESEARCH ARTICLE

A Compact Monopulse Antenna Array With Suppressed Mutual Coupling Using Broadband Schiffman Phase Shifters

SAEID ALAMDAR[1], (Graduate Student Member, IEEE), KARIM MOHAMMADPOUR-AGHDAM[2], (Member, IEEE), AND HOSSEIN KHALILI[2], (Graduate Student Member, IEEE)

[1]Department of Electrical Engineering and Computer Science, University of California at Irvine, Irvine, CA 92697, USA
[2]School of Electrical and Computer Engineering, College of Engineering, University of Tehran, Tehran 1417935840, Iran

Corresponding author: Saeid Alamdar (salamdar@uci.edu)

ABSTRACT This study presents the design, fabrication, and measurement of a compact microstrip monopulse antenna array for surveillance applications. The design process and limitations of the planar antenna structure are discussed, including the stacking of two radiating elements as a parasitic loaded patch antenna to increase bandwidth and suppress mutual coupling. A distributed feeding network for 8×16 elements with an integrated monopulse comparator, was designed and optimized, with the comparator placed in a separate layer to prevent spurious radiation. The operating frequency is 15.5-18 GHz, and the antenna exhibited a bandwidth of approximately 15%. The measurement results for the fabricated antenna array align with the simulations and design goals, with sidelobe levels of the beam better than 17 dB in both the E- and H-plane, and a null depth in the Delta pattern of less than -30 dB. The peak gain at the operating frequency is 22.3 dB and the total efficiency of the antenna array is approximately 55%.

INDEX TERMS Microstrip antenna array, monopulse comparator, mutual coupling, null depth, Schiffman phase shifter.

I. INTRODUCTION

A monopulse tracker system is defined as one that obtains the angular position of a target by comparing the signals received in simultaneous Sigma and Delta beams. The use of simultaneous beams is a key advantage of monopulse systems because it avoids amplitude changes over time. Traditional monopulse systems commonly employ Cassegrain parabolic antennas, reflect arrays, or lens antennas [1], [2]. In some cases, a five-element horn feed capable of independently optimizing Sigma and Delta was realized [3]. Additionally, multimode horns that utilize TE_{11} mode for Sigma and higher order waveguide modes, such as TE_{21} or TM_{01}, for generating Delta-beams from a single aperture, have been reported [4], [5]. These antennas offer high efficiency and independent optimization of Sigma and Delta modes. However, these antennas are not suitable for low-profile and small-volume structures, which are often required in surveillance systems because of their size and weight limitations [6].

Planar monopulse comparators traditionally utilized 180° hybrid couplers like rat-races [7] for their design. However this solution presents challenges in integrating 180°, 3 dB hybrid couplers into planar circuits, particularly concerning the positioning of SUM and DELTA ports, and the impracticality of integrating with the antenna array's feeding network. In response, the use of 90°, 3 dB hybrid couplers along with 90° delay line phase shifters has become a common way to mimic the performance of 180° hybrid couplers and achieve monopulse functionality [8], [9], [10],

The associate editor coordinating the review of this manuscript and approving it for publication was Raghvendra Kumar Chaudhary.

[11], [12]. Unfortunately, the inclusion of additional 90° phase shifters introduces undesired dispersion in the monopulse comparator, restricting the 30 dB null bandwidth to less than 6%. To overcome this limitation and extend the null bandwidth, Barker and Rebeiz [13] used a 0-dB coupler to guide signals without coupling, eliminating the need for two 90° delay lines in two hybrids. This modification resulted in an expanded 30 dB null bandwidth, reaching 20% for one of the DELTA channels, while the bandwidth for other channels remained unchanged. A symmetrical uni-planar monopulse comparator by cascading two identical 90° couplers with two phase delay lines, where the total phase delay of two lines is 180° is also presented in [14] achieving 20 dB null depth with 8% bandwidth. In our effort to further enhance the 30 dB null bandwidth, a new architecture for monopulse comparators was designed. This innovative design incorporates interconnected branchline 3 dB hybrid couplers alongside wideband improved Schiffman phase shifters, instead of conventional delay line phase shifters. As a result, we achieved a 20% 30 dB null bandwidth in both DELTA channels within the monopulse comparator and a 15% 30 dB null bandwidth when integrated with the antenna array. This study employs an innovative design that incorporates four broadband branch-line couplers and multiple 90° phase shifters using multistage Schiffman coupled-lines [15]. This approach achieves both compact size and wideband capability.

The comparator's construction and performance evaluation were conducted separately through fabrication and measurement processes. The schematic of the proposed monopulse antenna array is shown in Fig. 1. In this figure, the antenna array is divided into four symmetric quadrants, and each quadrant is then connected to the monopulse comparator with a specific phase shift. The monopulse antenna has four ports; Sigma, Delta1, Delta2, and Delta3. At the Sigma port, the power from each array quadrant are summed in phase. At the Delta1 port, array quadrants A and B are summed in phase, and array quadrants C and D are summed in phase. These two signals were then subtracted from each other to produce a null in the horizontal plane. Similarly, at port Delta2, quadrants A and C are summed in phase, and quadrants B and D are summed in phase. Again, these two signals are subtracted from each other to produce a null in the vertical plane. Port Delta3 was not used and was connected to a 50-ohm load.

Previous studies have documented various microstrip monopulse antennas. Our study aimed to enhance the existing knowledge base by introducing an innovative 8 × 16 antenna array. Our focus is on exploring the implications of monopulse antennas in the context of large antenna array designs. A compact microstrip monopulse antenna array in the Ku-band, in a single layer, was proposed in [8], but with a narrow bandwidth of less than 5.6 % and demonstrated the effects of spurious radiation and blockage on sidelobe levels caused by the comparator. A broadband multilayer microstrip antenna with ratrace hybrid couplers and parasitic patches over the air gap in the X-band was implemented to

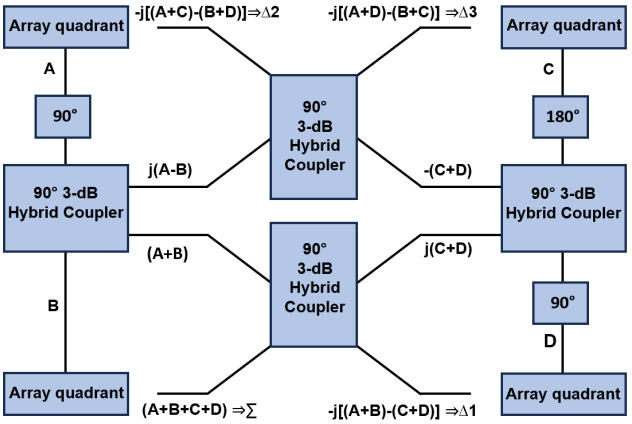

FIGURE 1. Schematic structure of the proposed monopulse antenna array using the 90° 3-dB hybrid couplers.

increase the realized gain in [7], a four-element antenna with ratrace hybrid couplers was also presented in [11], and, a 1-D electronic beam-scanning monopulse antenna array based on a compact stripline phase-shifter was introduced in [16]. the concept of using stripline phase-shifter is also used to design Series-Fed Monopulse Microstrip Antenna array in [12]. A 4×4 broadband planar microstrip monopulse antenna array with a monopulse comparator in a separate layer has been reported in the C-band, which utilizes dual-layer patches with an air gap to enhance the antenna bandwidth [10]. A one-dimensional low-sidelobe-level monopulse antenna using miniaturized ring couplers in the S-band was reported in [17]. A reconfigurable antenna with Sigma and Delta patterns for WLAN access points was presented in [18] A 2 × 2 reconfigurable monopulse antenna with controllable polarization is also presented in [19]. More recently, substrate integrated waveguide (SIW) technology has been applied in millimeter-wave antenna design, such as a 6×8 microstrip aperture-coupled patch antenna array with a SIW-based feeding network in the V-band [20].A 2 × 2 dual-polarized monopulse antenna in X band was also presented in [21]. SIW slot antenna arrays have also been proposed [22], [23], [24]. Although SIW technology combines the advantages of planar transmission lines and non-planar waveguides, it is more susceptible to fabrication tolerances because of the dependence of the phase constant on the permittivity of the substrate.

The monopulse antenna array discussed in this paper consists of three main components: radiating elements, feeding network, and monopulse comparator. Section II provides an overview of the required specifications and introduces the proposed antenna structure. In Section III, a wideband antenna element is designed, and its operational bandwidth is improved using two-layered microstrip patches and parasitic elements. Section IV focuses on the design of a distributed feeding network for an 8 × 16 element array, with the aim of achieving low sidelobe levels in both the E- and H-planes for the Sigma radiation pattern.

In Section V, a monopulse comparator is designed, which includes interconnecting 3-dB 90° hybrid couplers and improved Schiffman phase shifters. Finally, the designed components are aggregated, and the overall antenna array structure is subjected to a full-wave simulation in Section VI. Subsequently, the antenna array is fabricated and measured to validate its performance in Section VII.

II. SPECIFICATIONS AND STRUCTURE OF ANTENNA ARRAY

The specifications of this monopulse antenna array are as follows:

- Operating frequency range: 15.5-18 GHz
- Antenna array bandwidth: 15%
- Sigma-Delta ports isolation < 23 dB
- Polarization: linear
- Sidelobe level of Sigma Patterns(SLL) < -17 dB
- Null depth of Delta patterns < -30 dB
- Half-power beamwidth in E-plane: 5 degrees
- Half-power beamwidth in H-plane: 10 degrees
- The maximum gain: 22.3 dBi
- Array size: 8 × 16 elements
- Size of the antenna: 130 mm × 240 mm

The 8×16 antenna array was split into symmetrical quadrants to obtain monopulse operation. The outputs of the elements in each quadrant are summed to produce four signals that are then combined to form a Sigma, Delta1 in H-plane or Azimuth, and Delta2 in E-plane or Elevation. To satisfy the beamwidth requirements, each quadrant was formed using 4×8 radiators with a parallel feed network. The quadrants were interconnected to the four ports of the monopulse comparator. The comparator had four input ports and four output ports. Four input ports are connected to four quadrants, and four output ports are connected to Sigma, Delta1 (in azimuth), Delta2 (in elevation), and an isolated port terminated at a 50 Ω load. The ground plane separates the patch antennas and the feeding network to eliminate any negative effects of the feeding network, such as spurious radiation, and blockage of the comparator.

III. DESIGN OF THE RADIATING ELEMENT

A resonant rectangular patch is the basic configuration of a microstrip patch antenna. However, when used in an array configuration, typical patch antennas suffer from a narrow bandwidth and high mutual coupling, which are major disadvantages. To overcome these limitations, several studies have been conducted to improve its design. One common solution is the use of stacked patches, which enhance the bandwidth without significantly increasing the size of the antenna structure [25], [26]. Another approach is to place additional parasitic elements next to the patch, which are electrically disconnected from the central patch, but have a significant coupling with the driven patch owing to the electromagnetic fringing fields associated with the patches. By adjusting the length of the parasitic elements, the resonant frequency was slightly displaced from the driven patch, thereby increasing the bandwidth. Parasitic structures are also used to reduce mutual coupling between two patches in a narrow bandwidth [27]. As shown in Fig. 2, the design of the proposed patch antenna comprises four steps. The first step involves designing a pin-fed rectangular patch antenna that operates at the desired center frequency. In the second step, another rectangular patch is added on top of the first one to introduce another resonance in the input impedance, thus broadening the bandwidth. The third step involves the incorporation of two rectangular parasitic elements into the stacked patch antenna. These parasitic elements are not physically connected to the patch antenna but are excited through the coupling between the driven patch and parasitic elements. These parasitic elements, along with the stacked patch, can add another resonance to the input impedance, thereby contributing to the broadening of the bandwidth. In the final step, the driven patch and parasitic elements were shaped and dented to obtain additional design parameters to enhance the bandwidth and suppress the mutual coupling between the driven patch antenna and adjacent patch antennas.

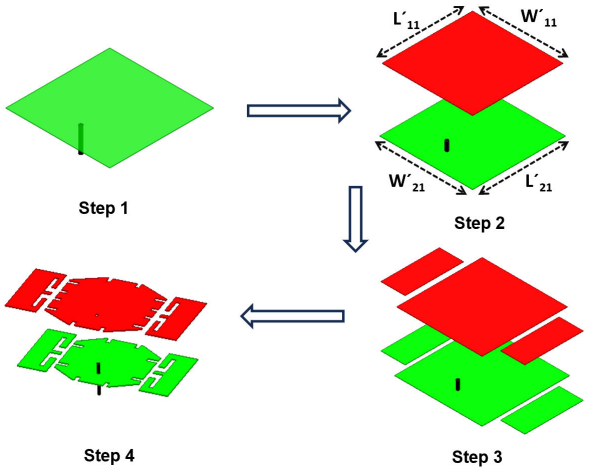

FIGURE 2. The design steps for the proposed patch antenna, (dimensions: W'_{11}=4.5 mm, W'_{21}=4.2 mm, L'_{11}=4 mm, L'_{21}=3.8 mm).

The optimized stacked patch antenna with parasitic elements, as shown in Fig. 3, achieves a wide operating bandwidth while suppressing mutual coupling with neighboring antennas in an array configuration.

In addition to its function as a radiating element, the parasitic element was utilized as a coupling element to counteract mutual coupling between patches. By introducing an additional coupling path, the parasitic element cancels out the original coupling, thus improving isolation [28], [29]. To illustrate the effectiveness of the coupling element in enhancing the isolation, Fig. 4 presents a comparison of the surface current distribution between the proposed patch antenna and a rectangular stacked patch antenna. As indicated, when the left patch is excited, the current induced on the neighboring patch (right) of the proposed

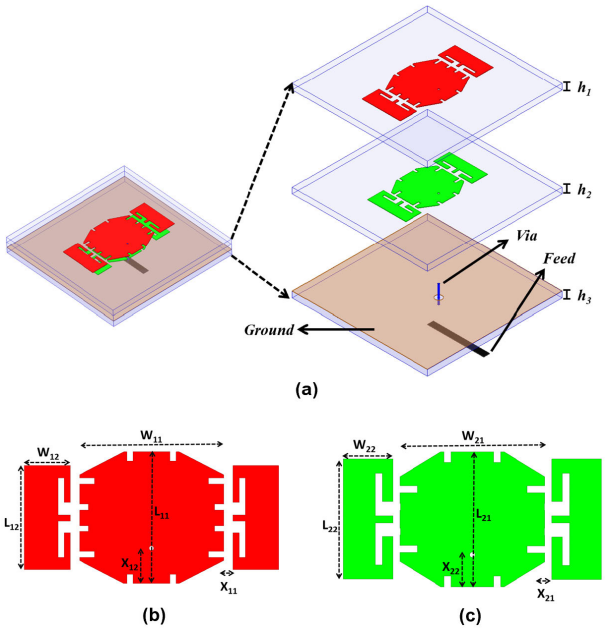

FIGURE 3. Proposed patch antenna (a) exploded view, (b) upper patch, (c) lower patch, (dimensions: W_{11} =4.5 mm, W_{21} =4.2 mm, L_{11} =3.9 mm, L_{21} =3.6 mm, W_{12} =1.2 mm, W_{22} =1 mm, L_{12} =2.9 mm, L_{22} =2.6 mm, X_{11} =0.2 mm, X_{12} =0.2 mm, X_{12} =1.2 mm, X_{22} =1 mm, $h_1 = h_2 = h_3$ =0.508 mm).

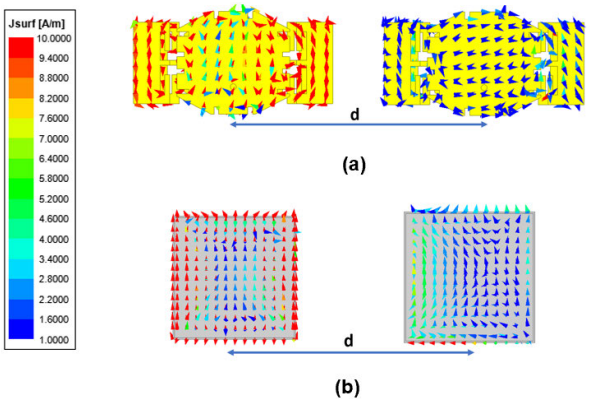

FIGURE 4. Surface current distribution on neighbor patch (right), while main patch (left) is excited (a) proposed stacked parasitic loaded patch, and (b) rectangular stacked rectangular patch (d=14 mm).

element is significantly reduced compared with that of the stacked rectangular patch.

A comparison of the simulated reflection coefficient between the proposed patch antenna and the basic stacked rectangular patch antenna, the dimensions of which are illustrated in step 2 of Fig. 2, is illustrated in Fig. 5. By incorporating two parasitic elements and optimizing their length, shape and distances from the driven patch, the bandwidth was increased from 12% for the basic stacked rectangular patch antenna to 20% for the proposed patch antenna without causing significant pattern distortions. The simulated isolation with the neighboring patch antenna for both the optimized patch antenna and the basic rectangular

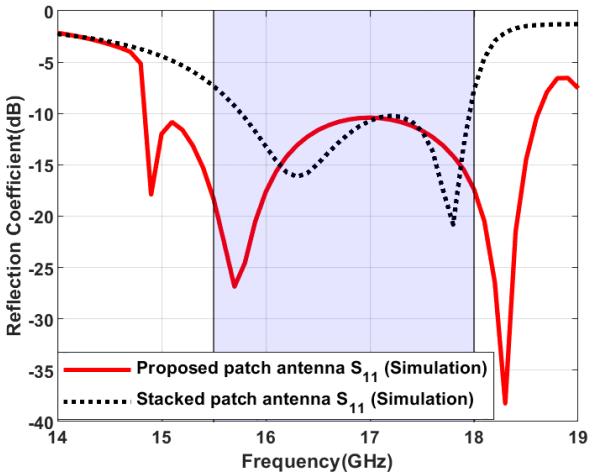

FIGURE 5. Comparison of reflection coefficient bandwidth between the proposed antenna and a basic rectangular stacked antenna.

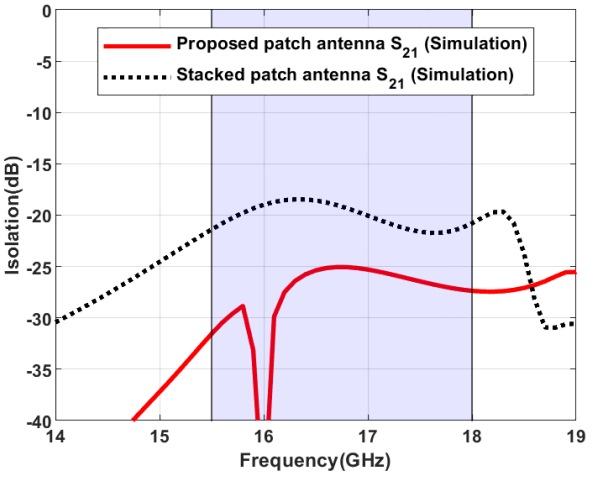

FIGURE 6. Comparison of isolation between the proposed antenna and a basic rectangular stacked antenna.

stacked patch antenna is depicted in Fig. 6. The results of the parametric studies indicate that careful adjustment of the basic design parameters can lead to a reduction of more than 5 dB in the mutual coupling between two antennas over the required bandwidth.

IV. FEEDING NETWORK DESIGN

The symmetric design of the antenna allows the design of a feed network in only one of the 4×8 quadrants. The feed network was connected to each stacked patch using vias. To achieve a non-uniform amplitude distribution in the feed network, T-junction power dividers were employed, with the power divider ratio determined by the ratio of each arm's impedance. The design procedure for T-junctions is provided in [29]. the optimization of the T-junction power dividers in the 4×8 quadrant feed network was achieved using Keysight ADS, where a penalty function was defined to optimize each T-junction ratio. The feed network was then simulated using

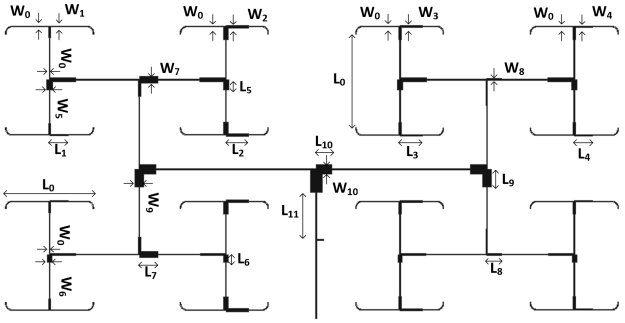

FIGURE 7. The geometry of T-junction power divider (W_0 =0.15 mm, W_1 =0.18 mm, W_2 =0.47 mm, W_3 =0.26 mm, W_4 =0.21 mm, W_5 =0.9 mm, W_6 =0.75 mm, W_7 =1 mm, W_8 =0.31 mm, W_9 =1.38 mm, W_{10} =1.48 mm, L_0 =14 mm, L_1 =2.94 mm, L_2 =3.62 mm, L_3 =3.53 mm, L_4 =2.94 mm, L_5 =1.62 mm, L_6 =1.19 mm, L_7 =2.99 mm, L_8 = 2.31 mm, L_9 =2.86 mm, L_{10} =2.48 mm, L_{11} =2.51 mm.

a full-wave simulator, and an optimized design was obtained by repetitively building the feed network. This method significantly reduced the computation time. To satisfy the required sidelobe level, which should be better than −17 dB, a Taylor distribution was applied on both the E-plane and H-planes. The primary optimization objective was to maximize the gain of the Sigma beam while maintaining a low sidelobe level. This goal was achieved by ensuring that the weighting magnitude error for each antenna element was less than 0.5 dB, and the weighting phase error was kept within ±5 degrees. The optimized feeding network for each quadrant and its dimensions are shown in Fig. 7.

V. DESIGN OF MONOPULSE COMPARATOR

The monopulse comparator is a crucial component of the antenna system that combines four inputs from the quadrants to generate Sigma and Delta signals. A schematic of the proposed monopulse comparator is shown in Fig. 8. In this particular design, the monopulse comparator reported in [15] was used. It is composed of four branchline 90° 3dB hybrid couplers and four wideband Schiffman 90° phase shifters. A cascade of two 90° phase shifters is employed to achieve a 180° phase shift. A photograph of the fabricated monopulse comparator is shown in Fig. 9. The design procedure for this monopulse comparator is described in detail in [15].

The characteristics of the monopulse comparator were measured using a vector network analyzer(VNA). S-parameter files were used to calculate the insertion loss and null depth for both Delta channels. The results of the evaluation using the simulation and measurement S-parameters of the Sigma port are shown in Fig. 10. The insertion loss is between -1.5 dB to -2.5 dB in the Sigma channel passband.

To measure the null depth of the monopulse comparator, a total of 16 two-port measurements were performed. During each two-port measurement, the remaining six ports were terminated with a 50Ω load. Subsequently, the S-parameter files were used to calculate the null depth at both DELTA1

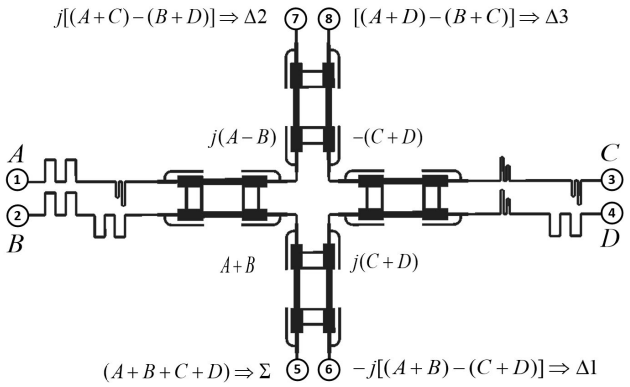

FIGURE 8. Schematic structure of the proposed monopulse comparator [15].

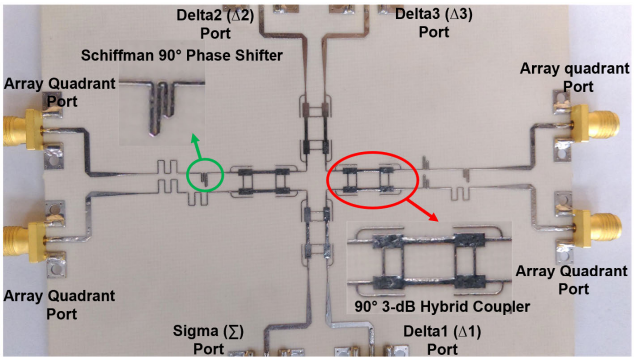

FIGURE 9. Photograph of the fabricated monopulse comparator [15].

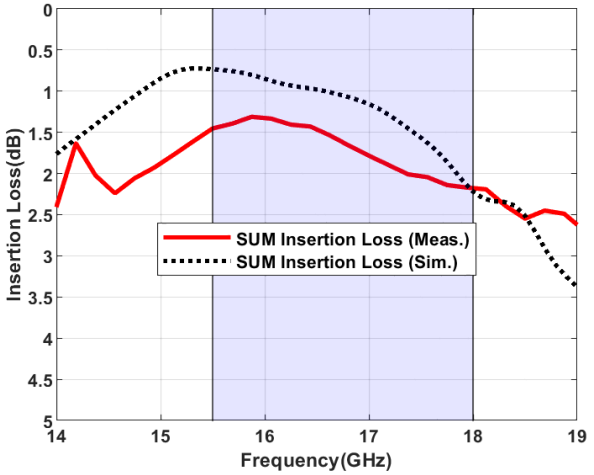

FIGURE 10. Comparison of simulated and measured comparator insertion loss.

and DELTA2 using Equations (1) and (2), respectively.

$$\text{Delta1} = 20\log\left(\frac{S_{(\Delta1,1)}+S_{(\Delta1,2)}+S_{(\Delta1,3)}+S_{(\Delta1,4)}}{S_{(\Sigma,1)}+S_{(\Sigma,2)}+S_{(\Sigma,3)}+S_{(\Sigma,4)}}\right) \quad (1)$$

$$\text{Delta2} = 20\log\left(\frac{S_{(\Delta2,1)}+S_{(\Delta2,2)}+S_{(\Delta2,3)}+S_{(\Delta2,4)}}{S_{(\Sigma,1)}+S_{(\Sigma,2)}+S_{(\Sigma,3)}+S_{(\Sigma,4)}}\right) \quad (2)$$

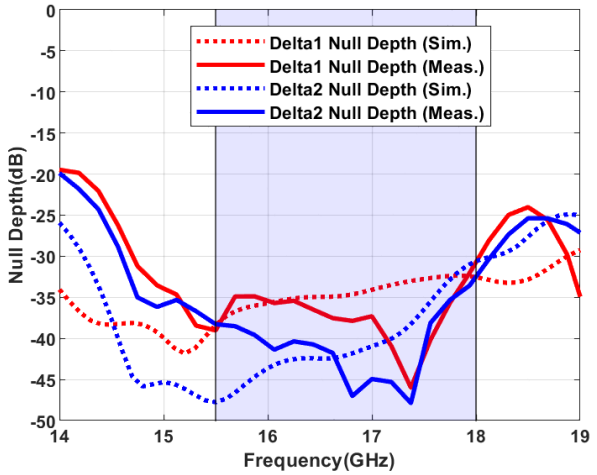

FIGURE 11. Comparison of simulated and measured comparator null depth.

Which the expression

$$S_{(\Delta j,i),i=1,2,3,4,j=1,2}$$

denotes the S-parameter at ports Delta1 or Delta2 from each array quadrant. And the expression

$$S_{(\Sigma,i),i=1,2,3,4,}$$

denotes the S-parameter at port Sigma from each array quadrant.

Ideally, the summation of the power received from the four quadrants at ports Delta1 and Delta2 should be zero. However, because of the non-ideality of 90° hybrid couplers and phase shifters, this summation is not zero. Because of the semi-symmetry of the monopulse structure, it is reasonable that the null depth results for DELTA1 and DELTA2 are similar to each other. This is evident in Fig. 11, where the simulation results for Delta1 and Delta2, as well as the measurement results for Delta1 and Delta2, exhibit similarity. Due to the non-idealities introduced by fabrication errors, the measured null depth for Delta1 and Delta2 is higher than the simulation null depth. Nevertheless, in both simulation and measurement results, the null depths at Delta1 and Delta2 were consistently below -30 dB within the desired frequency range of 15.5-18 GHz.

VI. PUTTING IT ALL TOGETHER

Finally, the designed radiating elements, feed network, and monopulse comparator are integrated and simulated using a full-wave simulator. Subsequently, a prototype of the proposed monopulse antenna is fabricated, and photographs of the prototype are presented in Fig. 12.

VII. RESULTS AND DISCUSSIONS

The radiation patterns, realized gain, Voltage Standing Wave Ratio (VSWR), and port isolation of the antenna have been measured. The measurement setups, utilizing a Vector

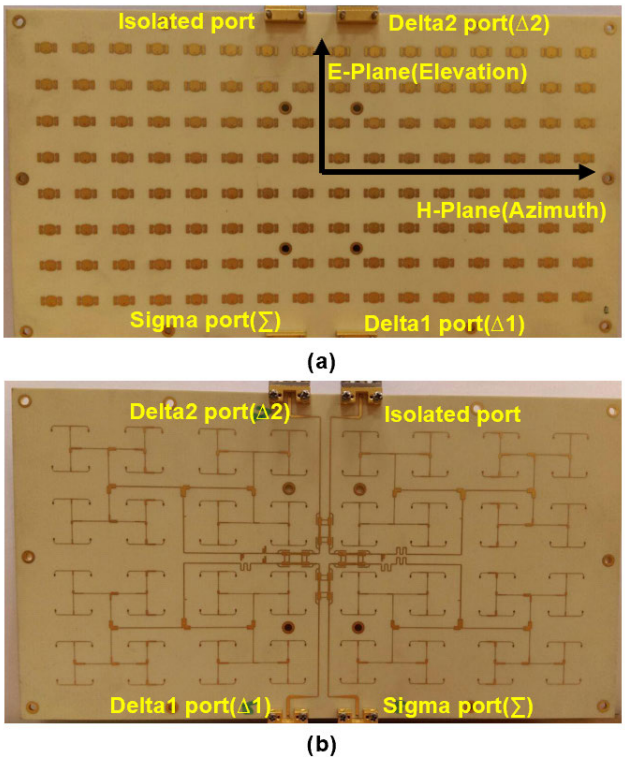

FIGURE 12. Photograph of the prototype of monopulse antenna (a) top view, (b) bottom view.

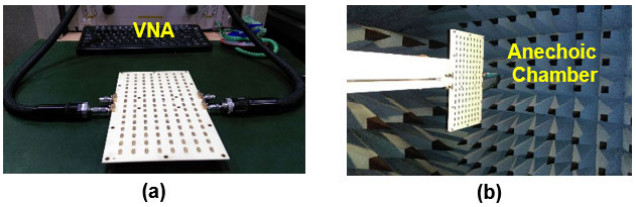

FIGURE 13. Measurement set-up for (a) S-parameters, and (b) radiation patterns and gain.

Network Analyzer (VNA) for S-parameter measurements and positioning the antenna in an anechoic chamber for gain and radiation pattern measurements, are illustrated in Fig. 13. The VSWR measurements for the Sigma and Delta ports are presented in Fig. 14. For the VSWR measurement of each port (Sigma, Delta1, and Delta2), the other ports were terminated with a 50Ω load. We can observe that for the Sigma port, the VSWR is below 1.7 in the frequency range of 15.5-18 GHz. For Delta1 and Delta2, the VSWR is below 2 and 2.1, respectively, in the desired frequency range.

Additionally, Fig. 15 shows the isolation between each pair of ports. The isolation between Sigma and Delta 1 is below 23 dB, and that between Sigma and Delta2 is less than 26 dB. The isolation between Delta1 and Delta2 is also less than 30 dB

A gain-comparison method was used to measure the gain of the antenna in an anechoic chamber. A comparison of the simulated and measured realized gain for the sigma port

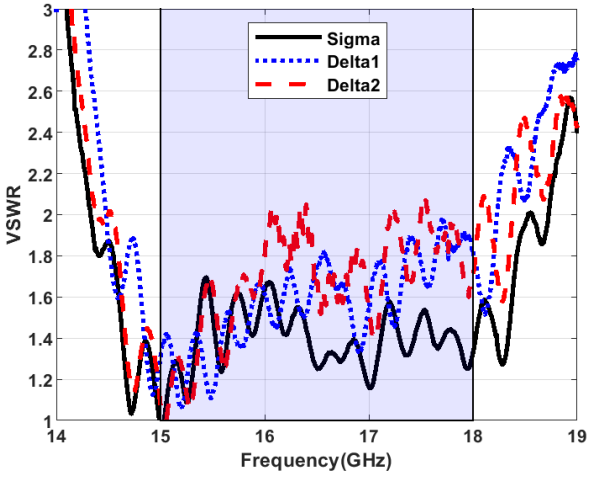

FIGURE 14. Measured VSWR.

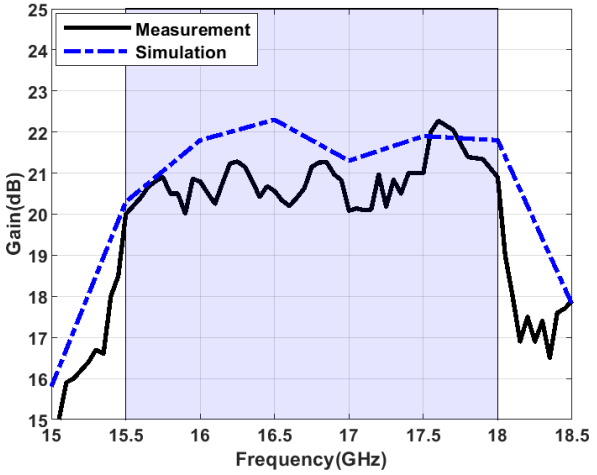

FIGURE 16. Comparison of simulated and measured gain of Sigma beam.

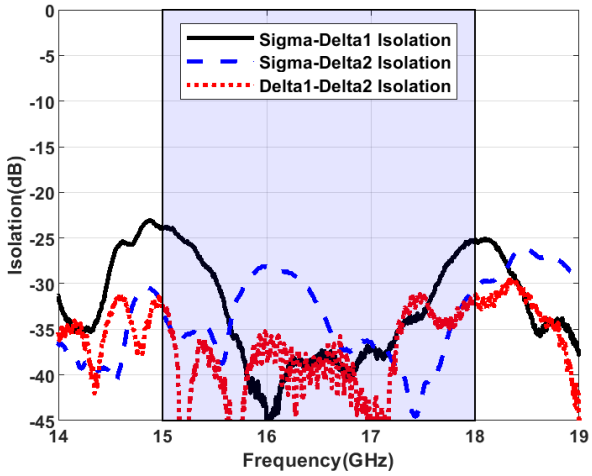

FIGURE 15. Measured isolation between ports.

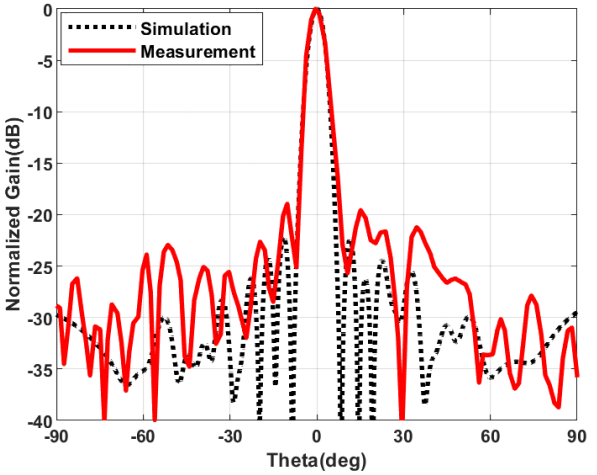

FIGURE 17. Comparison of the simulated and measured Sigma radiation pattern in H-Plane.

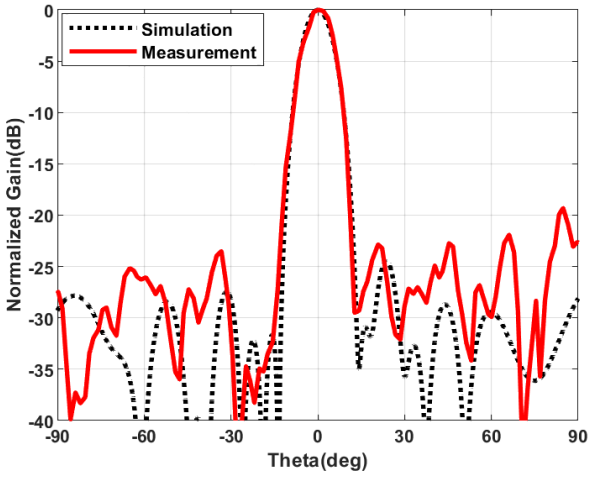

FIGURE 18. Comparison of the simulated and measured Sigma radiation pattern in E-Plane.

of the antenna array is shown in Fig. 16. The peak of the Sigma beam gain is up to 22.3 dB, which is comparable to the simulated realized gain. The measured efficiency of the antenna array is approximately 55%, which is lower than that of a conventional microstrip antenna array because of the losses associated with the monopulse comparator circuit.

The monopulse antenna array investigated in this study generates a Sigma beam in both the E- and H-planes (elevation and azimuth, respectively) when excited at the Sigma port. The Sigma radiation patterns in both planes were measured at the center frequency. The H-plane (horizontal) radiation pattern of the Sigma port is shown in Fig. 17, indicating a beamwidth of 5.5° and a SLL of less than 17 dB. Similarly, the E-plane (vertical) radiation pattern of the Sigma port is shown in Fig. 18, demonstrating a beamwidth of 11° and a SLL of less than 23 dB.

Fig. 19 and Fig. 20 illustrate the H-plane and E-plane DELTA radiation patterns, respectively at the center frequency. The null depths in both planes are less than -30 dB, which is comparable to the measured null depth of the comparator depicted in Fig. 11. In Table 1, we provide a comparison between our proposed novel monopulse antenna

TABLE 1. Comparison between this work and previous works.

Ref	Freq. band	bandwidth(%)	Size(λ_0)	Number of elements	Null depth(dB)	SLL(dB)	Comparator design
[7]	X	21	6.7×6.7	8×8	-35	-15	ratrace
[8]	Ku	5.6	13.5×12.5	16×16	-30	-17	branch-line couplers with delay lines
[11]	X	2.1	1.6×1.8	2×2	-27	-19*	ratrace
[12]	Ka	2.8	16.9×15.75	80×4	-30	-24	branch-line coupler with delay lines
[14]	C	8	1.95×1.5	2×2	-20	-15*	Symmetric coupler + zero-phase crossover
[19]	X	50	Not provided	2×2	-48	-18*	branch-line coupler with delay lines
This work	Ku	15	7.2×13.4	8×16	-32	-17	branch-line couplers with Schiffman phase shifters

* The beamwidth is wide due to the number of antenna elements.

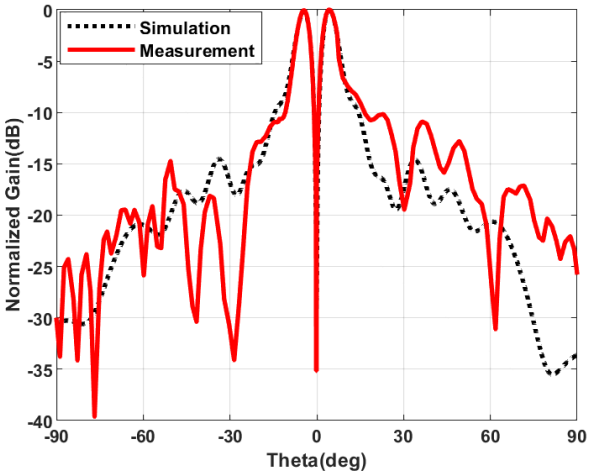

FIGURE 19. Comparison of the simulated and measured Delta radiation pattern in H-Plane.

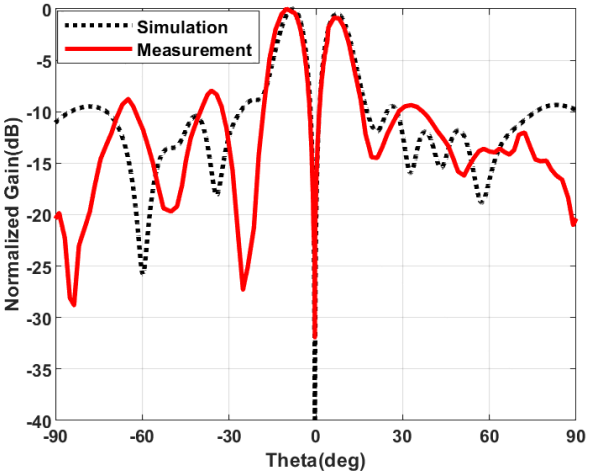

FIGURE 20. Comparison of the simulated and measured Delta radiation pattern in E-Plane.

array, which incorporates a monopulse comparator with Schiffman phase shifters, and previously reported planar microstrip antennas.

VIII. CONCLUSION

This paper proposes a broadband monopulse antenna array at the Ku-band that effectively suppresses mutual coupling between antenna elements. The design steps and performance predictions presented in this study can serve as guidelines for designing low-cost microstrip monopulse antennas. The measured results confirm that the antenna meets high-level specification requirements. The antenna has a bandwidth of 15%, achieving a measured peak gain of 22.3 dB. The total efficiency of the antenna is approximately 55%, and the null depths in both the E-plane and H-plane are less than -30 dB. This antenna is expected to be useful for low-cost, lightweight monopulse surveillance applications.

REFERENCES

[1] P. Zheng, B. Hu, S. Xu, and H. Sun, "A W-band high-aperture-efficiency multipolarized monopulse Cassegrain antenna fed by phased microstrip patch quad," *IEEE Antennas Wireless Propag. Lett.*, vol. 16, pp. 1609–1613, 2017.

[2] D. N. Black and J. C. Wiltse, "Millimeter-wave characteristics of phase-correcting Fresnel zone plates," *IEEE Trans. Microw. Theory Techn.*, vol. MTT-35, no. 12, pp. 1122–1129, Dec. 1987.

[3] S. S. Roy, C. Saha, T. Nagasekhar, S. B. Mane, C. S. Padmavathy, G. Umadevi, and M. N. Kumar, "Design of a compact multielement monopulse feed for ground-station satellite tracking applications," *IEEE Antennas Wireless Propag. Lett.*, vol. 18, no. 9, pp. 1721–1725, Sep. 2019.

[4] S. M. M. Azizi and S. H. Mohseni Armaki, "A compact TE_{21} mode coupler for tracking purposes," *IEEE Microw. Wireless Compon. Lett.*, vol. 28, no. 6, pp. 470–472, Jun. 2018.

[5] J. R. Montejo-Garai, J. A. Ruiz-Cruz, and J. M. Rebollar, "Design of a Ku-band high-purity transducer for the TM_{01} circular waveguide mode by means of T-type junctions," *IEEE Access*, vol. 7, pp. 450–456, 2019.

[6] M. Alesheikh, R. Feghhi, F. M. Sabzevari, A. Karimov, M. Hossain, and K. Rambabu, "Design of a high-power Gaussian pulse transmitter for sensing and imaging of buried objects," *IEEE Sensors J.*, vol. 22, no. 1, pp. 279–287, Jan. 2022.

[7] H. Kumar and G. Kumar, "Broadband monopulse microstrip antenna array for X-band monopulse tracking," *IET Microw., Antennas Propag.*, vol. 12, no. 13, pp. 2109–2114, Oct. 2018.

[8] H. Wang, D.-G. Fang, and X. G. Chen, "A compact single layer monopulse microstrip antenna array," *IEEE Trans. Antennas Propag.*, vol. 54, no. 2, pp. 503–509, Feb. 2006.

[9] B. Liu, W. Hong, Z. Kuai, X. Yin, G. Luo, J. Chen, H. Tang, and K. Wu, "Substrate integrated waveguide (SIW) monopulse slot antenna array," *IEEE Trans. Antennas Propag.*, vol. 57, no. 1, pp. 275–279, Jan. 2009.

[10] Z.-W. Yu, G.-M. Wang, and C.-X. Zhang, "A broadband planar monopulse antenna array of C-band," *IEEE Antennas Wireless Propag. Lett.*, vol. 8, pp. 1325–1328, 2009.

[11] S. A. Khatami, J. Meiguni, A. Amn-e Elahi, and P. Rezaei, "Compact via-coupling fed monopulse antenna with orthogonal tracking capability in radiation pattern," *IEEE Antennas Wireless Propag. Lett.*, vol. 19, no. 8, pp. 1443–1446, Aug. 2020.
[12] L. Zou, X. Wang, and J. Zang, "Series-fed monopulse microstrip array antenna with stripline quadrature hybrid comparator network," *IEEE Access*, vol. 9, pp. 169177–169192, 2021.
[13] N. S. Barker and G. M. Rebeiz, "An octave bandwidth monopulse processor," in *IEEE MTT-S Int. Microw. Symp. Dig.*, Denver, CO, USA, 1997, pp. 1213–1215.
[14] H. Zhang, H. Ren, Y. Gu, and B. Arigong, "A fully symmetrical uni-planar microstrip line comparator network for monopulse antenna," *IEEE Microw. Wireless Technol. Lett.*, vol. 33, no. 5, pp. 611–614, May 2023.
[15] S. Alamdar, K. Mohammadpour-Aghdam, H. Khalili, and M. Mohammad-Taheri, "A miniaturized broadband monopulse comparator with all DELTA channels nulling in ku band," *Int. J. Microw. Wireless Technol.*, vol. 10, no. 9, pp. 1035–1041, Aug. 2018.
[16] H.-J. Zhao, H. Chu, X. Zhu, and Y.-X. Guo, "A 1-D electronic beam-scanning monopulse antenna array based on a compact stripline phase-shifter," *IEEE Antennas Wireless Propag. Lett.*, vol. 19, no. 12, pp. 2477–2481, Dec. 2020.
[17] X. Nie, W. Hong, and K. Fan, "Monopulse array and low side-lobe level array with a novel feed network," *IET Microw., Antennas Propag.*, vol. 12, no. 12, pp. 1978–1985, Oct. 2018.
[18] H. Sun, X. Ge, W. He, and L. Zhao, "A reconfigurable antenna with sum and difference patterns for WLAN access points," *IEEE Antennas Wireless Propag. Lett.*, vol. 19, no. 7, pp. 1073–1077, Jul. 2020.
[19] S. Karamzadeh, "Polarization diversity controllable monopulse antenna array design," *IEEE Access*, vol. 11, pp. 7078–7084, 2023.
[20] T. Mikulasek, J. Lacik, J. Puskely, and Z. Raida, "Design of aperture-coupled microstrip patch antenna array fed by SIW for 60 GHz band," *IET Microw., Antennas Propag.*, vol. 10, no. 3, pp. 288–292, Feb. 2016.
[21] Z. Sun, S. Liu, Y. Yang, X. Zheng, J. Wang, W. He, T. An, and X. Zhao, "A dual-polarized 2-D monopulse antenna array based on substrate integrated waveguide," *IEEE Trans. Antennas Propag.*, vol. 70, no. 12, pp. 11771–11778, Dec. 2022.
[22] Y. J. Cheng, W. Hong, and K. Wu, "94 GHz substrate integrated monopulse antenna array," *IEEE Trans. Antennas Propag.*, vol. 60, no. 1, pp. 121–129, Jan. 2012.
[23] Y. J. Cheng, W. Hong, and K. Wu, "Design of a monopulse antenna using a dual V-type linearly tapered slot antenna (DVLTSA)," *IEEE Trans. Antennas Propag.*, vol. 56, no. 9, pp. 2903–2909, Sep. 2008.
[24] W. Li, S. Liu, J. Deng, Z. Hu, and Z. Zhou, "A compact SIW monopulse antenna array based on microstrip feed," *IEEE Antennas Wireless Propag. Lett.*, vol. 20, no. 1, pp. 93–97, Jan. 2021.
[25] S. D. Targonski, R. B. Waterhouse, and D. M. Pozar, "Design of wide-band aperture-stacked patch microstrip antennas," *IEEE Trans. Antennas Propag.*, vol. 46, no. 9, pp. 1245–1251, Sep. 1998.
[26] R. B. Waterhouse, "Design of probe-fed stacked patches," *IEEE Trans. Antennas Propag.*, vol. 47, no. 12, pp. 1780–1784, Dec. 1999.
[27] H. Wang, D. G. Fang, and P. Ge, "Mutual coupling reduction between two conformal microstrip patch antennas," in *Proc. 5th Asia–Pacific Conf. Environ. Electromagn.*, Xi'an, China, Sep. 2009, pp. 176–179.
[28] A. Habashi, J. Nourinia, and C. Ghobadi, "Mutual coupling reduction between very closely spaced patch antennas using low-profile folded split-ring resonators (FSRRs)," *IEEE Antennas Wireless Propag. Lett.*, vol. 10, pp. 862–865, 2011.
[29] G. R. Branner, B. Preetham Kumar, and D. G. Thomas, "Design of microstrip T junction power divider circuits for enhanced performance," in *Proc. 38th Midwest Symp. Circuits Systems. Proc.*, Rio de Janeiro, Brazil, 1995, pp. 1213–1215.

SAEID ALAMDAR (Graduate Student Member, IEEE) received the B.S. degree in electrical engineering from the Isfahan University of Technology, Isfahan, Iran, in 2014, and the M.S. degree from the University of Tehran, Tehran, Iran, in 2017. He is currently pursuing the Ph.D. degree with the University of California at Irvine, Irvine, CA, USA.

From 2017 to 2021, he was associated with the Antenna Type Approval Laboratory, University of Tehran, as a Research Assistant. He was an Intern with NXP Semiconductors, from Summer 2023 to Fall 2023. His research focuses on flexible printed circuits, antennas on chips, antenna arrays, and intelligent reconfigurable reflects arrays (IRA or RIS).

KARIM MOHAMMADPOUR-AGHDAM (Member, IEEE) received the B.S. degree in electrical engineering from the Sharif University of Technology, in 2001, the M.S. degree from the University of Tehran, in 2003, and the Ph.D. degree from the School of Electrical and Computer Engineering, University of Tehran, in 2011.

He joined the School of Electrical and Computer Engineering, University of Tehran, as an Assistant professor. Before starting the Ph.D. study, he was with the University of Tehran, as a Research Assistant, to establish the Antenna Type Approval Laboratory, where has been a Technical Manager of the Laboratory. In 2008, he was admitted as the Ph.D. Student with KU Leuven, Belgium, to work on sponsored projects by IMEC, including RFID and mm-wave measurement systems. In 2022, he joined WaveCORE KU Leuven, as a Visiting Professor. During the past 12 years, he has supervised more than 20 bachelor's and 45 master's or doctoral graduated students. He has co-founded a successful start-up company with the University of Tehran Science and Technology Park, in 2016, which currently has more than 400 employees and is one of the main players in the private sector. He is active in the development of cellular communication products and public access to the internet. His general research interests include applied electromagnetics, microwave and mm-wave imaging and remote sensing systems, miniaturized integrated antennas and radio sensors, and modeling and optimization of microwave and mm-wave devices.

HOSSEIN KHALILI (Graduate Student Member, IEEE) was born in Tabriz, Iran, in 1991. He received the B.S. degree in telecommunication engineering from Tabriz University, Tabriz, in 2014, and the M.S. degree in telecommunication engineering from the University of Tehran, Tehran, Iran, in 2017. He is currently a Research Assistant with the Antenna Type Approval Laboratory, University of Tehran. His current research interests include antenna arrays, array pattern synthesis, neural networks, deep learning, and radar imaging.